Assessment of Noise Reduction of Hyperspectral Imagery using a Target Detection Application

Shen-En Qian*[a], Josée Lévesque[b] and Reza Rashidi Far[a]
[a]Canadian Space Agency, 6767 Route de l'Aeroport, St-Hubert, QC, Canada J3Y 8Y9
[b]Defence Research and Development Canada, 2459 Boul. Pie-XI N., Québec, QC, Canada G3J 1X5

Abstract

This paper is an evaluation of a previously proposed noise reduction technology for hyperspectral imagery to examine whether it could help to better serve remote sensing applications after noise reduction using the technology. Target detection from hyperspectral imagery is selected as an example for the evaluation. A hyperspectral datacube acquired using the airborne Short-wave-infrared Full Spectrum Image II (SFSI-II) with man-made targets deployed in the scene of the datacube was tested. In addition to an evaluation using receiver operating characteristic (ROC) curve approach, this paper uses a spectral un-mixing technique to generate the fraction images of the target materials, then measures the area of the targets derived from the datacube before and after applying the noise reduction technology and compares the derived target areas to the real targets to assess the detectability of the targets. The area ratio between a derived target and the real target is used as the criterion in the evaluation. The evaluation results showed that the noise reduction technique can help to better serve remote sensing applications. The small targets that cannot be detected from the original datacube were detected after the noise reduction using the technology.

1. Introduction

Designing and building a satellite sensor with a considerably higher signal-to-noise ratio (SNR) is a challenge, as high SNR could be prohibitively expensive and constrained by technology availability. For example, in Phase A study of the Canadian Hyperspectral Environment and Resource Observer (HERO) satellite, the study concluded that the SNR of HERO will be 600:1[1]. However, some of the HERO users require data with SNR of 1000:1 in order to derive their application products. Motivated by this requirement and the challenge, a novel technology improving SNR of hyperspectral data by removing noise in the data using wavelet based denoising technology has been developed and reported (Othman and Qian, 2006). Figure 1 shows the block diagram of the noise reduction technology that removes noise using a hybrid spectral-spatial noise reduction (HSSNR) approach. Experimental results show that the HSSNR can improve SNR of hyperspectral imagery up to 98% for the test data sets.

The effectiveness of the HSSNR noise reduction technology needs to be assessed using remote sensing algorithms and applications. A simplified application-based evaluation was conducted on a short wave infrared (SWIR) data set for target detection applications (Qian et al., 2006a). Spectral angle mapper (SAM) and end-members of different target materials were used. The end-member spectrum of a target material was used as the seed spectrum to match the spectra of the pixels of a target of that material to measure the derived area of the target for assessing the detectability of the target before and after applying the HSSNR noise reduction technology. The experimental results show that small targets, which cannot be detected in the original data set due to inadequate SNR and low spatial resolution, are more likely to be detected after the noise of the data set is reduced.

*Corresponding author. Email address: shen-en.qian@asc-csa.gc.ca

[1]SNR at 650 nm with 30% albedo and 30° solar zenith angle

Othman and Qian (2008) have carried out an evaluation of the noise reduction technology using intermediate remote sensing products. They adopted two approaches to evaluating the hyperspectral data sets that are denoised using the technology. The first approach evaluated the effectiveness of the noise reduction technology using narrow band vegetation indices and red-edge positions of the hyperspectral data sets, while the second approach evaluated the effectiveness using a number of spectral similarity measures. Evaluation results show that the HSSNR noise reduction technology yielded comparable results to existing denoising technologies for vegetation indices, red-edge positions and superior results for spectral similarity measures. The detailed evaluation results of the intermediate remote sensing products have been reported by Othman and Qian (2008).

This paper evaluates the effectiveness of the HSSNR noise reduction technology using a remote sensing application. Target detection is selected as an example for the purpose of examining whether the noise reduction technology could help to better serve remote sensing applications. A hyperspectral data set with man-made targets deployed in the scene of a short wave infrared (SWIR) data set was tested. Spectral un-mixing is used in the detection of the targets. End-members of different target materials and their corresponding fraction images were produced and used to evaluate the detectability of the targets derived from the data set before and after applying the noise reduction technology.

Target detection from hyperspectral imagery has been an active research area since 1990's. Hyperspectral target detection algorithms can be basically classified into two categories: spectral-only and spectral-spatial. The spectral-only algorithms use the known spectral signatures of the targets (Manolakis et al., 2000). This category of algorithms includes the spectral matched filter (Crist et al., 1999), the SAM (Haskett and Sood, 1997), and linear mixture models (Grossmann et al., 1998; Chang et al., 1998; Slater and Healey, 1998). The spatial-spectral algorithms apply when there is no known target spectral signature (Manolakis et al., 2000). They locate pixels that display different spatial and/or spectral characteristics from their surroundings. The spatial-spectral algorithms can be further divided into local anomaly and global anomaly detectors (Masson and Pieczynski, 1993; Ferrara, 1994; Yu et al., 1997; Schowengerdt, 1997; Ashton, 1998; Jain, 1998; Stocker, 1999; Schweizer and Moura, 2001).

The target detection algorithm used in this paper is of spectral-only, as the spectral signatures of the targets are known. Olsen et al (1997) used SAM and matched filter techniques to detect and identify targets from hyperspectral data in an area consisting of grassy fields and forest areas. A variety of targets were deployed in the field with ground truth spectra. They reported that both the techniques were successful in locating targets, but the matched filter seemed to suffer more from "false positives", though this may have been a function of thresholds set in the classification process. Achal et al (1999) demonstrated the feasibility of detecting surface-laid and, in some circumstances, buried mines from visible to near-infrared hyperspectral imagery using linear correlation coefficient and orthogonal subspace projection. When the detection is defined to be a cluster of between 2 and 5 pixels exceeding the threshold of the classified image, the probability of detection of individual mines is 100% without false alarms. If the detection condition is relaxed to include single pixels above threshold, 12 false alarms are present. Manolakis et al (2003) made an overview of the theoretical and practical issues associated with the development, analysis, and application of target detection algorithms for hyperspectral image data. They described design, evaluation and taxonomy of target detection in hyperspectral image data. They also described the detectors for full-pixel targets and for sub-pixel targets. They derived the basic algorithms in each family, explained how they work, and provide results for their theoretical performance. Kwon and Nasrabadi (2004) employed a non-linear matched filter for target detection in hyperspectral imagery. They showed that the non-linear matched filter could easily be implemented using the ideas of kernel functions and the non-linear matched filter outperforms the linear version. Glenn et al (2005) used mixture tuned matched filter for repeat detection of small targets of invasive plant species from hyperspectral imagery. West (2005) studied the spectral matched filter of unstructured background characterization and evaluated up-to-date unstructured background characterization methods as well as some new methods that improve stochastic modeling of the background. Goovaerts et al (2005) reported approaches to detecting small targets in hyperspectral imagery: a multivariate statistical analysis of all spectral bands using PCA; a geostatistical filtering of noise and regional background in the first principal components using factorial kriging; and the computation of a local indicator of spatial autocorrelation to

detect local clusters of high or low reflectance values and anomalies. They concluded that the proposed approaches outperform traditional target detectors (i.e., the Mahalanobis distance based detectors) and fewer false alarms are obtained. Park et al (2007) adopted correlation coefficient as a measure of spectral characterization to detect targets from hyperspectral images and investigated the relationship between the number of spectral bands used and the performance of the detection process in order to find the optimal number of band reductions.

The subject of this paper is the assessment of the effectiveness of the developed noise reduction technology using target detection as an example of applications. Study of different target detection techniques from hyperspectral imagery is beyond the scope of this paper. This paper is organized as follows. The first section is the Introduction. In the next section, after the description of the test data set and the method of target detection using spectral un-mixing, the evaluation criterion is discussed. Then the evaluation results and analysis are presented. The conclusion is drawn in the last section.

2. Test Data Set and Evaluation Method

2.1 Test Data Set

In this paper the hyperspectral data set tested was acquired using the airborne Short wave infrared (SWIR) Full Spectrum Imager II (SFSI-II) (Neville et al., 1995) on June 7, 2002 at an altitude of 1800m with ground pixel size of 2.20m×1.85m, and 240 bands covering a spectral range between 1200 nm and 2450 nm with a band interval of 5 nm. The sky condition was clear with a few cirrus clouds. Pollen was also present in the air in a non-negligible amount.

This data set (also referred to as datacube in this paper) was acquired for studying target detection in SWIR hyperspectral imagery. Man-made targets with different materials and sizes were deployed in a mixed of sand and low-density grass cover within the image scene of the datacube. Seven pieces of awnings with varying sizes ranging from 12m×12m to 0.2m×0.2m, four pieces of polythene, four pieces of white tarp and four pieces of white cotton with varying size ranging from 6m×6m to 0.5m×0.5m were deployed. In addition, a 3m×3m piece of white tarp was placed on a large vinyl turf mat of size 11m×14m. The upper part of Figure 2 shows the layout of the man-made targets and the lower part shows the disposition of the targets on the ground viewed from an IKONOS panchromatic scene with 1m resolution. The man-made targets can be easily identified from the 1m-resolution IKONOS panchromatic image down to the size of 3m×3m. The 1.5m×1.5m awning target and the three 1m×1m targets of awning, white tarp and cotton materials on the right of the target array can be barely identified.

The acquired raw datacube was first pre-processed to remove periodic noise, dark current, slit curvature (also referred to as smile) and spatial distortion (also referred to as keystone). Then a vicarious calibration was performed to convert the raw data into radiance. No geo-correction is applied. The radiance data is stored as 16-bit values. The size of the datacube is 140 lines by 496 pixels per line by 240 bands.

2.2 Target Detection from Hyperspectral Data Using Spectral Un-mixing

Due to the datacube acquired by the SFSI-II sensor being in the shortwave infrared region (between 1200 nm and 2450 nm), it is difficult to distinguish the targets in the data from the infrared region datacube, even when visualized in (R, G, B) wavelengths visible to human eyes (see Figure 3 (a)). Since the spectral signatures of the target materials are known, spectral information based target detection algorithms can be applied. In this paper a traditional spectral un-mixing technique is used to generate the fraction image (also referred to as abundance image) for each of the target materials. As an example, Figure 3 (b) shows a part of the fraction image of the awning material. The pixels of targets of the awning material display with high fraction values in the awning fraction image. In this way the targets can be "distinguished." The fraction image of a target material can then be used to identify and detect the targets of that material. The endmember extraction algorithm and spectral un-mixing algorithm in the ISDAS (Imaging Spectrometer Data Analysis System)

software suite (Staenz et al., 1998) were used to generate the fraction images. In the evaluation of this paper, the targets of polythene material are excluded due to their unstable detectability. This is because the polythene is transparent. Targets of polythene material are mixed up with background and other materials. It is difficulty to identify polythene targets from the fraction images.

2.3 Evaluation Masks

The orientation of the man-made target array (as shown in the upper part of Figure 2) in the scene of the SFSI-II datacube is not well aligned with the airplane flight direction. There is a rotation of approximate 36^o between the target array and the cross-track line (perpendicular to airplane flight direction) of the SFSI-II datacube. Figure 4 shows the illustration of the target array in the scene of the SFSI-II datacube after being rotated by 36^o counter-clockwise.

In this paper, in order to evaluate the detectability of the targets derived from the test datacube, target masks were introduced and created. A target mask covers the pixels of a specific size target as much as possible. Figure 5 depicts the masks for the targets used in the evaluation of this paper. Factors have been taken into account in determining the centre location and the coverage area of each of the target masks. Due to the fact that the ground pixel size (spatial resolution) of the SFSI-II instrument is 2.20m×1.85m, the small targets occupy only a portion of a ground pixel (referred to as sub-pixel). The rotation angle between the scene of SFSI-II datacube and the target array makes the thing even more complicated. Figure 6 presents examples of ground pixels covered by a target of size 6m×6m, 3m×3m and 1m×1m when the target array has a rotation angle of 36^o to the cross-track line of the SFSI-II datacube. For a 6m×6m target as shown in the left graphics of Figure 6, the target occupies 13 pixels. There are only 3 pixels (i.e. *h*, *l* and *m*) that are "pure" pixels. Ten out of 13 are sub-pixels. For a 3m×3m target (centre graphics in Figure 6), it covers seven pixels (i.e. ***h,*** *l*, *m*, *n*, *q*, *r* and *s*) in the scene of the SFSI-II datacube. These pixels are all sub-pixels. The 1m×1m target (right graphics in Figure 6) covers four sub-pixels (i.e. *g*, *h*, *l* and *m*).

In order to accurately locate the centre of a target mask, the information created in an early evaluation study (Qian et al., 2006a) is utilized. The evaluation in the study used the endmember spectrum (*e*) of a target material as the seed spectrum to match the spectrum (*s*) of each of the pixels of the target to generate the spectral angles (i.e. $spectral\text{-}angle = \cos^{-1}(|e|.|s|)$) between the spectra of the endmember and each of the target pixels. The contours of spectral angle values can be used to assist in the determination of the centre of a target mask. The location of the pixel (or the centre of the pixels) whose spectrum has the smallest spectral angle to the endmember spectrum is very likely to be the centre of the target. In this paper this centre is used as the centre of the mask.

The coverage area of a target mask is determined by taking into account the facts of sub-pixels occupied by a target and of the possible shift of the mask centre to the real target centre caused by the inaccurate mask centre locating. An approximate two-pixel mis-locating margin is adopted in addition to the target area. For example, for a 1m×1m target (as shown in the right graphics in Figure 6), 4×4=16 pixels covering the rectangle area marked by the thick line box are selected as the coverage area of the mask. In this way, if the centre of the mask is inaccurately located caused by shifting to the real target centre by one pixel or maximum two pixels left, right, up or/and down, the mask still can cover the pixels occupied by the target. For a 3m×3m target (as shown in the centre graphics in Figure 6), 5×5=25 pixels within the thick box in the graphics are selected as the coverage area of the mask. The locations of the masks and their sizes (i.e. numbers of pixels) are given in Figure 5. In the figure, there is a 255-pixel shift to the original SFSI-II image for the cross-track pixel number.

The creation of the endmember spectra of the target materials is critical in the evaluation, as the endmember spectra directly influence the quality of the fraction images for deriving the targets from the datacube. There are two approaches to obtain the endmember spectra of the target materials. The first approach is to obtain the endmember spectra of the target materials from a spectral library or use ground spectra of the target materials. However, the spectra in spectral libraries and the ones collected on the ground can only be used in their reflectance form if they are compared with air-/space-borne spectra because of the

variations introduced by the atmosphere in the latter. This approach was not deemed possible since the test SFSI-II datacube is in radiance. The second approach is to obtain the endmember spectra of the target materials from the datacube itself. This is a widely used approach and adopted in this paper. Iterative Error Analysis (IEA) algorithm included in ISDAS software suite (Staenz et al., 1998) is used to extract endmembers from the datacubes before and after noise reduction. Using IEA, an endmember spectral array was thus created for each datacube, i.e. the original datacube and the noise reduced datacube. The endmember spectra of the awning and cotton materials derived from the original datacube and from the noise-reduced datacube using the HSSNR have been reported by Qian et al. (2006a). These spectra look very similar except the denoised spectra are smoother in the non-absorption peak regions.

2.4 Evaluation Criterion

Receiver operating characteristic (ROC) curves are widely used in target detection and the comparison of different target detection techniques. The more upward bowed ROC curve is, the higher the detectability. In our study, ROC curves of targets of awning, white tarp and cotton targets of size from 12m×12m to 3m×3m were created and analyzed. Figure 7 shows some of the ROC curves of the targets derived from the original SFSI-II datacube and the noise-reduced datacube using HSSNR. It can be seen from the figure that the ROC curves of the 6m×6m awning targets derived from the original SFSI-II datacube and the noise-reduced datacube are perfect. They are completely overlapped. The ROC curves of the 12m×12m awning target derived from the original and the noise-reduced datacubes are almost perfect and overlapped. The ROC curves of the 6m×6m white tarp and cotton targets derived the noise-reduced datacube show higher detectability than those derived from the original SFSI-II datacube. For the 3m×3m targets, the ROC curve of the awning target derived from the noise-reduced datacube is slightly higher than that derived from the original datacube, while the ROC curve of the cotton target derived from the original datacube is significantly higher than that derived from the noise-reduced datacube. These results indicate that the HSSNR noise reduction technology can help to increase the detectability of large targets. However, another approach is needed in order assess the noise reduction technology for the small target detection.

In this paper, we proposed to evaluate the detectability of the targets derived from the datacubes before and after noise reduction based on the target area ratio of a derived target versus the real target. The areas of the real targets in this paper are known (e.g. 144m^2 for a 12m×12m target and 36m^2 for a 6m×6m target), as they are man-made. The area of a derived target is a key measurement in the detection of the target. The closer the area of a derived target to the area of the real target, the better the detectability of the target. The area of a derived target can be estimated by counting the number of pixels of the target, as a ground pixel is equal to 2.20m×1.85m=4.07m^2 that is determined by the spatial resolution of the SFSI-II sensor. In reality, however, the target pixels under the mask are not all "pure" pixel of the material as shown in Figure 6. Most of target pixels under the mask are sub-pixels. In order to take into account the contribution of the sub-pixels to the target area, the fractions of all the pixels under the mask with respect to a particular material are summed. Then the sum fraction is used to estimate the number of full ("pure") pixels of the target. Every 100% fraction is counted as a full pixel of the target of the material. The criterion is defined as following:

$$Ratio\ of\ Target\ Area = \frac{\text{Sum of fractions of pixels of the derived target} \div 100 \times 4.07\, m^2}{\text{Area of the real target}} \quad (1)$$

In evaluation of an awning target, for example, the fraction image corresponding to the awning endmember (for awning material) is used. The fractions of pixels under the mask of the target in the awning fraction image are summed for calculating *Ratio-of-Target-Area*. The closer to 1 is the *Ratio-of-Target-Area*, the better the detectability of the derived target. Similarly for the targets of white tarp and cotton materials, the fraction images corresponding to white tarp and cotton materials are used.

3. Evaluation Results

This section presents the evaluation results using the criterion defined above. The detectability of the man-made targets derived from the original SFSI-II datacube and the datacube after noise reduction using HSSNR technology are assessed. A noise-reduced datacube using a smoothing based technique reported by Staenz et al (1998) is also assessed for the sake of comparison with the HSSNR noise reduction technology. The smoothing based noise-reduced technique was utilized in the applications of the SFSI-II data sets before the development of the HSSNR technology, such as in applications reported by Qian et al. (2005, 2006b). It removes random noise of the SFSI-II data by applying a spectral-spatial smoothing based on the known noise characteristics of the SFSI-II sensor. That is, it averages spectra from a number of different pixels that are equivalent based on the known noise characteristics of the sensor in the laboratory calibration. This noise removal technique can improve the data quality of SFSI-II data for remote sensing applications. As reported by Qian et al. (2006b), the H_2O band at 1470 nm and water vapour features in the radiance spectra of the SFSI-II datacube cannot be properly estimated before the random noise is removed using this technique. They can be well estimated from the radiance spectra after applying the smoothing based noise reduction technique.

The original datacube was undergone noise reduction using both the HSSNR and the smoothing algorithms. Then the original datacube and the noise reduced datacubes were de-striped, which is the last pre-processing before applying application algorithms. The IEA algorithm in ISDAS was used to extract the purest pixels from each of the datacubes as the endmembers. The number of endmembers to be extracted was set to 20, which is the number suggested by the developer. After extraction of the endmembers, the IEA reports the locations of the endmembers in the scene of the datacube. In this study, since the locations of the targets are known, the endmembers extracted by the IEA algorithm can be verified by the locations of the targets. The first observation was that some of the endmembers of the target materials were not obtained by IEA. The IEA found all the endmembers of the targets materials for the HSSNR datacube. The IEA did not find the endmember of cotton material for the original datacube. It did not find the endmembers of both cotton and white tarp materials for the smoothed datacube. Those missing endmembers were still missing when the upper limit number of endmembers (66 in the ISDAS software version used) was used.

Depending on the uncertainty on the available endmembers one can un-mix the datacube by fully constraining, weakly constraining or no constraining. While the fully constrained and no constrained imply the existence or non existence of the conditions during the un-mixing procedure, weakly constrained calculates the fraction images for those available endmembers but assumes not all of the fractions are known. This results in the fractions to be all between zero and one with their summation at each pixel between zero and one, contrary to the fully constrained un-mixing where they have to add up to one. In order to detect the targets derived from the datacube before and after noise reduction, the datacubes are un-mixed using the endmembers extracted from the datacubes themselves. The un-mixing is implemented in ISDAS. To compensate for those missed endmembers, a weakly constrained un-mixing was applied. The fraction images of the target materials are used in the assessment. As in some cases, more than one endmember was found for a target of a material, the corresponding fraction images for the endmembers were added together to form the fraction of the respective target.

Table 1 lists the nominal sum of fraction and obtained sum of fraction of the targets derived from the original datacube and the noise reduction datacubes using smoothing and HSSNR, as well as the area ratio of the derived targets to their real targets. Because the IEA did not find the endmember of cotton material for the original datacube and the endmembers of white tarp and cotton materials for the noise reduction datacube using smoothing, the sum of fraction of the targets for those endmembers are all listed as zero in the table. In the table, the Nominal Sum of Fraction is defined as:

$$\text{Nominal Sum of Fraction} = \frac{\text{real target area } (\text{m}^2)}{\text{nominal pixel area } (\text{m}^2)} \times 100 \,. \tag{2}$$

For example, for the 12×12 target, Nominal Sum of Fraction is equal to $\frac{12\times12\,(\mathrm{m}^2)}{4.07\,(\mathrm{m}^2)}\times100\% = 3538.1\%$.
It is the maximum sum of fraction of a target to be detected. In theory, the sum of fraction of a target should not exceed its nominal sum. It can be seen from the table that many sums of fraction obtained are greater than the nominal sum of fraction, especially for the small targets whose area ratio to the real target is up to 12.13 (0.2×0.2 awning target). These sums of fraction are problematic for the assessment.

There are many factors that affect the sum of fraction of a target. First of all, the noise (including many unknown interferences and error sources) in spectral un-mixing is the main factor. Second, purity of the endmembers is another factor. Third, the accuracy of un-mixing matrix calculation is also a factor. The current spectral un-mixing technology is established based on the assumption of linear mixture. In real life mixture of natural materials is not linear. In addition to these factors, the point spread function of the pixels also contributes to this problem. An isolated pixel of pure material never produces a 100% fraction due to its energy spread to the neighbouring pixels decided by its point spread function. A pixel with 30% coverage of a material to be detected (sub-pixel) never produces exactly 30% fraction of that material in real life.

In order to minimize the artefacts which are arisen as a result of the factors mentioned above, we conducted a post-processing to reduce the effect of the artefacts. We assume the artefacts act as "pollution" in this paper. In other words, each pixel in the datacube is polluted independently with the same probability. To cancel out this pollution, we remove the area that the targets exist from each of the fraction images. Then we calculate the average fraction for each fraction image of the endmembers. As there is no target in the target-removed fraction images, these average fractions reveal the pollution fraction per pixel of the datacube for each endmember. Now using these pollution fractions, one can modify the fraction images over the target area. Assuming the pollution fraction for endmember i is r_i , the corresponding fraction, c_i , is modified as follows:

$$\hat{c}_i = c_i - r_i \,. \tag{3}$$

Table 2 lists the pollution fraction for each of the endmembers of the original datacube and the noise reduced datacubes using smoothing and HSSNR. Again, the pollution fractions of cotton material for the original datacube and of white tarp and cotton materials for the noise reduction datacube using smoothing are set to zero in the table due to IEA did not find the endmembers for them. The pollution fractions of the HSSNR datacube are lower than those of the original datacube for the same materials, especially of the white tarp material (0.78% vs. 2.01%), which indicates that the HSSNR technique suppressed the noise somewhat. The pollution fractions of the smoothed datacube are inconsistent for the two detected materials. The pollution fraction of the awning material is worse than that of the original datacube, whereas the pollution fraction of the vinyl material is lower than both the original and the HSSNR datacubes.

Let's look at the sum of fractions after the removal of the pollution fraction. Table 3 lists the adjusted sum of fractions of the targets derived from the original datacube and the noise reduction datacubes using smoothing and HSSNR. Since the removal of the pollution fraction from the obtained sum of fraction is a subtraction operation, the adjusted sums of fraction of the targets will be in negative if the pollution fraction is greater than the target fraction. It can been seen from the adjusted sum of fractions that, in general, the areas of the targets derived from the noise reduced datacube using HSSNR are closer to the real targets than those derived from the original and the noise reduced datacube using smoothing. There is no negative sum of fraction for the targets derived from the noise reduced datacube using HSSNR after removal of the pollution. The sums of fraction for the targets derived from the original and the smoothed datacubes contain negative after removal of the pollution.

For awning targets, there are seven targets of size varying form 12m×12m to 0.2m×0.2m. The targets of size 0.5m×0.5m and 0.2m×0.2m are not detectable in this study. This is because their nominal sum of fraction is 6.1% and 1.0% respectively, while their sum of pollution fraction under their mask is 9×1.58%=14.22% and 4×1.58%=6.32% respectively when taking into account per pixel pollution fraction of

the awning endmember 1.58%. The sum of pollution fraction of these targets is greater than the nominal sum of fraction. That is why the area ratios of these two targets derived from the original and the noise reduced datacubes are so large or negative (between -6.55 and 5.68) even though the pollution fraction having been removed. The two rows of their results are shaded in the table to indicate that they are not reliable and for information only. For the 12m×12m awning target, whose nominal sum of fraction is 3538.1%, the sum of fraction derived from the original, smoothed and HSSNR datacubes is 2947.4%, 2588.0% and 2506.1% respectively. They correspond to area ratio to the real target 0.83, 0.73 and 0.99 respectively. The HSSNR datacube produces almost the perfect target area ratio (0.99). For the 6m×6m awning target, the area ratio is 0.94, 0.85 and 1.07 respectively for the target derived from the three datacubes. The original datacube produces 0.06 less area ratio to the full area ratio of this target, while the HSSNR datacube produces 0.07 more area ratio to the full. For the 3m×3m awning target, the area ratio is 0.65, 0.20 and 0.72 respectively for the target derived from the three datacubes. The HSSNR datacube produces the closest area ratio for this target among the three datacubes. The smoothed datacube produces the lowest area ratio (0.20). For the 1.5m×1.5m awning target, the area ratio is 1.14, 0.81 and 0.96 respectively for the target derived from the three datacubes. The area of the target derived from the HSSNR datacube is quite close to the real target. The original datacube produces an extra area ratio of 0.14. For the 1m×1m awning target, the smoothed datacube does not detect it, as the sum of fraction is negative. The original datacube produces a target area ratio of 0.60 and the HSSNR datacube produces a target area ratio of 1.13, which is 0.13 over to the real target area.

For the white tarp targets, the IEA did not find the endmember from the noise reduced datacube using smoothing. The 6m×6m is the largest target of white tarp material. The area ratio of this target is 0.87 and 1.02 derived from the original and the HSSNR datacubes respectively. The HSSNR datacube produces almost the perfect area ratio to the real target with only 0.02 over to the full ratio. For the 3m×3m, target, the area ratio is 1.16 and 1.35 respectively for the target derived from the two datacubes. These area ratios are all over to the full area by 0.16 and 0.35 respectively. For the 1m×1m white tarp target, the original datacube does not detect it, as the sum of fraction is negative. The HSSNR datacube produces an area ratio of 1.52 to the real target, which is 0.52 over to the full ratio.

For the cotton targets, the IEA did not find the endmembers from both the original datacube and the noise reduced datacube using smoothing. The HSSNR datacube produces an area ratio of 1.08, 0.30 and 0.11 respectively for the 6m×6m, 3m×3m and 1m×1m targets.

For the vinyl mat target, the three datacubes produce an area ratio of 1.08, 1.12 and 1.28 respectively. These area ratios are all over to the real target area, with the target derived from the original being closest to the real target area.

4. Discussion and Conclusion

This paper evaluates the effectiveness of a previously proposed noise reduction technology – Hybrid Spectral-Spatial Noise Reduction (HSSNR) – using a target detection application of a hyperspectral datacube acquired using the Short wave infrared Full Spectrum Imager II (SFSI-II) for studying target detection of hyperspectral imagery. In the scene of the datacube, man-made targets of different sizes and materials were deployed. In addition to an assessment using receiver operating characteristic (ROC) curve approach, this paper measures the area of the targets derived from the datacube before and after applying the noise reduction technology and compares the derived target areas to the real targets to assess the detectability the targets. The area ratio between a derived target and the real target is used as a criterion. The closer to one is the area ratio of a derived target, the better the detectability of the target.

In estimation of the area of a derived target, the sum of fractions of the pixels of the target is calculated in order to take into account the contribution of the pixels that occupy only a part of the target (sub-pixels) to the target area. The so-called "pollution" fraction per pixel is estimated for each fraction image to reduce the effects caused by noise and other negative factors of the un-mixing technology.

Table 4 summarizes the assessment results. In the table, the detection of a target is quantized to "yes", if the area ratio of the target is greater than 0.5. The detection of a target is quantized to "marginally", if the area ratio of the target is greater than 0 and less than 0.5. The detection of a target is quantized to "no", if the area ratio of the target is negative, or the IEA did not find the endmember for that target material. The area ratios of the targets are still included in the table for precise information of how good or bad a target is detected.

Table 4 clearly demonstrates that all the targets derived from the noise reduced datacube using HSSNR are detected or marginally (for the two cotton targets of size 3m×3m and 1m×1m) detected with a relatively closer to one area ratio. Meanwhile the targets derived from the original datacube are detected with a relatively poorer area ratio. All cotton targets are missed. Small targets of white tarp and awning are missed or poorly detected. These results indicate that HSSNR noise reduction technique could help to better serve remote sensing applications.

In this paper, a noise removal technique that is based on a spectral-spatial smoothing approach is also assessed for the sake of comparison to the HSSNR noise removal technology. The experimental results show that the targets derived from the datacube using this noise reduction technique are not well detected, especially for the small targets. This is probably caused by the nature of the noise reduction technique. This technique removes noise by using a spectral-spatial smoothing approach that might damages some subtle signature of the spectra.

Acknowledgements

The authors would like to thank the three anonymous reviewers for their valuable comments that help to improve the quality of this paper. The authors also thank Lixin Sun at Canada Centre for Remote Sensing for his help in using the ISDSA software and the Space Technology Research and Development Program (STRP) of the Canadian Space Agency for financial support.

References

Achal, S. B., Anger, C. D., McFee, J. E., and Herring, R. W. 1999, Detection of surface-laid mine fields in VNIR hyperspectral high spatial resolution data. *Proceedings SPIE*, vol. 3710, pp.808-818.

Ashton, E. 1998, Detection of subpixel anomalies in multispectral infrared imagery using an adaptive Bayesian classifier. *IEEE Transactions on Geoscience and Remote Sensing*, vol. 36, pp. 506–517.

Chang, C.-I., Zhao, X.-L., Althouse, M. L. G., and Pan, J. J. 1998, Least squares subspace projection approach to mixed pixel classification for hyperspectral images. *IEEE Transactions on Geoscience and Remote Sensing*, vol. 36, pp. 898–912.

Crist, E., Schwartz, C., and Stocker, A. 1999, Pairwise adaptive linear matchedfilter Algorithm. *Proc. DARPA Adaptive Spectral Reconnaissance Algorithm Workshop*.

Ferrara, C. F. 1994, Adaptive spatial/spectral detection of subpixel targets with unknown spectral characteristics. *Proceedings SPIE*, vol. 2235, pp.82–93.

Glenn, N.F., Mundt, J.T., Weber, K.T., Prather, T.S., Lass L.W., and Pettingill, J. 2005, Hyperspectral data processing for repeat detection of small infestations of leafy spurge, *Remote Sensing of Environment*, vol. 95, pp. 399–412.

Goovaerts, P., Jacquez, G. M., and Marcus, A. 2005, Geostatistical and local cluster analysis of high resolution hyperspectral imagery for detection of anomalies. *Remote Sensing of Environment*, vol. 95, pp. 351–367.

Grossmann, J., Bowles, J., Haas, D., Antoniades, J., Grunes, M., Palmadesso, P., Gillis, D., Tsang, K., Baumback, M., Daniel, M., Fisher, J., and Triandaf, I. 1998, Hyperspectral analysis and target detection system for the adaptive-spectral reconnaissance program (ASRP). *Proceedings SPIE*, vol. 3372, pp. 2–13.

Haskett, H. T., and Sood, A. K. 1997, Adaptive real-time endmember selection algorithm for sub-pixel target detection using hyperspectral data. *Proceedings 1997 IRIS Specialty Group Camouflage, Concealment, Deception*.

Hollinger, A., Bergeron, M., Maszkiewicz, M., Qian, S.-E., Staenz, K., Neville, R.A., and Goodenough, D.G. 2006, Recent Developments in the Hyperspectral Environment and Resource Observer (HERO) Mission. *Proceedings IGARSS'2006 IEEE International Geoscience and Remote Sensing Symposium*, pp.1620-1623.

Jain, A. K. 1998, *Fundamentals of Digital Image Processing*. Englewood Cliffs, NJ: Prentice-Hall, Ch. 2: Two Dimensional Systems and Mathematical Preliminaries.

Kwon, H., and Nasrabadi, N.M. 2004, Hyperspectral Target Detection Using Kernel Spectral Matched Filter. *Proceedings of Conference on Computer Vision and Pattern Recognition Workshop (CVPRW'04)*, Vol 8, pp.127-130.

Manolakis, D., Shaw, G., and Keshava, N. 2000, Comparative analysis of hyperspectral adaptive matched filter detectors. *Proceedings SPIE*, vol. 4049, pp.2-17.

Manolakis, D, Marden, D., and Shaw, G.A. 2003, Hyperspectral Image Processing for Automatic Target Detection Applications. *Lincoln Laboratory Journal*, vol. 14, No. 1, pp.79-116.

Masson P., and Pieczynski, W. 1993, SEM algorithm and unsupervised statistical segmentation of satellite images *IEEE Transactions on Geoscience and Remote Sensing*, vol. 31, pp. 618–633.

Neville, R.A., Rowlands, N., Marois R.V., and Powell, I. 1995, SFSI: Canada's first airborne SWIR imaging spectrometer. *Canadian Journal of Remote Sensing*, vol. 21, no. 3, pp. 328-336.

Olsen, R. C., Bergman, S., and Resmini, R. G. 1997, Target detection in a forest environment using spectral imagery. *Proceedings SPIE*, vol. 3188, pp.46-56.

Othman H., and Qian, S.-E. 2006, Noise Reduction of Hyperspectral Imagery Using Hybrid Spatial-Spectral Derivative-Domain Wavelet Shrinkage. *IEEE Transactions on Geoscience and Remote Sensing*, vol. 44, pp.397-408.

Othman H., and Qian, S.-E. 2008, Evaluation of Wavelet Denoised Hyperspectral Data for Remote Sensing. *Canadian Journal of Remote Sensing*, vol. 34, Supplement 1, pp. 59-67.

Park, K. S., Hong, S., Park, P., and Cho, W.-D. 2007, Spectral Contents Characterization and Analysis for Efficient Image Detection Algorithm Design, *EURASIP Journal of Applied Signal Processing*, vol. 2007, Article ID 82874, 14 pages, doi:10.1155/2007/82874.

Qian, S.-E., Bergeron, M., Lévesque, J., and Hollinger, A. 2005, Impact of Pre-processing and Radiometric Conversion on Data Compression Onboard a Hyperspectral Satellite. *Proceedings IEEE International Geoscience and Remote Sensing Symposium 2005*, Vol. 2, pp.700-703.

Qian, S.-E., Othman, H., and Lévesque, J. 2006a, Spectral Angle Mapper based Assessment of Detectability of Man-made Targets from Hyperspectral Imagery after SNR Enhancement. *Proceedings SPIE*, vol. 6361, pp.1-8 (63611H).

Qian, S.-E., Lévesque, J., and Neville, R.A. 2006b, Effect of Removing Random Noise of Radiance Data Using Smoothing on Data Compression Onboard a Hyperspectral Satellite. *WSEAS Transactions on Systems,* Issue 1, vol. 5, pp. 219-224.

Slater D., and Healey, G. 1998, Exploiting an atmospheric model for automated invariant material identification in hyperspectral imagery. *Proceedings SPIE*, vol. 3372, pp. 60–71.

Staenz, K., Szeredi, T., and Schwarz, J. 1998, ISDAS – A System for Processing/Analyzing Hyperspectral Data. *Canadian Journal of Remote Sensing*, Vol. 24, No. 2, pp. 99-113 (Also available at http://ccrs.nrcan.gc.ca/radar/ana/isdas_e.php).

Schowengerdt, R. A. 1997, *Remote Sensing: Models and Methods for Image Processing*. New York: Academic.

Schweizer, S.M., and Moura, J.M.F. 2001, Efficient Detection in Hyperspectral imagery. *IEEE Transactions on Image Processing*, Vol. 10, No 4, pp. 584-597.

Stocker, A. 1999, Stochastic expectation maximization (SEM) algorithm," *Proceedings DARPA Adaptive Spectral Reconnaissance Algorithm Workshop*.

West, J.E. 2005, Matched Filter Stochastic Background Characterization for Hyperspectral Target Detection. M.S. Degree Thesis of Rochester Institute of Technology, USA.

Yu, X., Hoff, L. E., Reed, I. S., Chen, A. M., and Stotts, L. B. 1997, Automatic target detection and recognition in multiband imagery: A unified ML detection and estimation approach. *IEEE Transactions on Image Processing*, vol. 6, pp. 143–156.

Table 1 Nominal sum of fraction and obtained sum of fraction of the targets derived from the datacubes before and after applying noise reduction as well as the area ratio of the derived targets to their real targets (without removal of the pollution fraction).

Material	**Target Size**	**Nominal Fraction Sum**	**Original**		**Noise Reduced Using Smoothing**		**Noise Reduced Using HSSNR**	
			Obtained Fraction Sum	Area Ratio	Obtained Fraction Sum	Area Ratio	Obtained Fraction Sum	Area Ratio
Awning	12mx12m	3538.1	3198.5	0.90	3135.6	0.89	3753.3	1.06
	6mx6m	884.5	885.4	1.00	876.9	0.99	1005.2	1.14
	3mx3m	221.1	183.0	0.83	132.5	0.60	198.5	0.90
	1,5mx1,5m	55.3	88.6	1.60	101.1	1.83	78.4	1.42
	1mx1m	24.6	40.5	1.65	18.7	0.76	53.2	2.16
	0,5mx0,5m	6.1	48.1	7.84	51.6	8.40	44.3	7.21
	0,2mx0,2m	1.0	0.0	0.00	9.3	9.46	11.9	12.13
White Tarp	6mx6m	884.5	838.1	0.95	0.0	0.00	927.6	1.05
	3mx3m	221.1	306.3	1.39	0.0	0.00	318.6	1.44
	1mx1m	24.6	27.8	1.13	0.0	0.00	49.9	2.03
Cotton	6mx6m	884.5	0.0	0.00	0.0	0.00	1052.1	1.19
	3mx3m	221.1	0.0	0.00	0.0	0.00	133.4	0.60
	1mx1m	24.6	0.0	0.00	0.0	0.00	45.4	1.85
Vinyl Mat	11mx14m	3783.8	5015.5	1.33	4566.2	1.21	5714.3	1.51

Table 2 Pollution fractions per pixel corresponding to the target endmembers derived from the original datacube and the noise reduced datacubes using smoothing and HSSNR

	Original	Noise Reduced Using Smoothing	Noise Reduced Using HSSNR
Awning	1.61	3.51	1.58
White Tarp	2.01	0.0	0.78
Cotton	0.0	0.0	2.67
Vinyl	8.25	2.87	7.52

Table 3 Sum of fraction of the targets derived from the datacubes before and after applying noise reduction as well as the area ratio of the derived targets to their real targets (after removal of the pollution fraction).

Material	Target Size	Nominal Fraction Sum	Original		Noise Reduced Using Smoothing		Noise Reduced Using HSSNR	
			Fraction Sum	Area Ratio	Fraction Sum	Area Ratio	Fraction Sum	Area Ratio
Awning	12mx12m	**3538.1**	2947.4	0.83	2588.0	0.73	3506.1	0.99
	6mx6m	**884.5**	827.4	0.94	750.5	0.85	948.2	1.07
	3mx3m	**221.1**	142.8	0.65	44.8	0.20	158.9	0.72
	1,5mx1,5m	**55.3**	62.8	1.14	44.9	0.81	53.1	0.96
	1mx1m	**24.6**	14.8	0.60	-37.5	-1.52	27.8	1.13
	0,5mx0,5m	**6.1**	33.7	5.48	20.0	3.25	30.0	4.89
	0,2mx0,2m	**1.0**	-6.4	-6.55	-4.7	-4.78	5.6	5.68
White Tarp	6mx6m	**884.5**	765.8	0.87	0.0	0.00	899.5	1.02
	3mx3m	**221.1**	256.1	1.16	0.0	0.00	299.1	1.35
	1mx1m	**24.6**	-4.4	-0.18	0.0	0.00	37.4	1.52
Cotton	6mx6m	**884.5**	0.0	0.00	0.0	0.00	956.1	1.08
	3mx3m	**221.1**	0.0	0.00	0.0	0.00	66.7	0.30
	1mx1m	**24.6**	0.0	0.00	0.0	0.00	2.8	0.11
Vinyl Mat	11mx14m	**3783.8**	4075.3	1.08	4239.0	1.12	4857.4	1.28

Table 4 Summary of detectability of the targets derived from the datacube before and after applying the HSSNR and the smoothing noise reduction techniques

Material	Target Size	Original		Noise Reduced Using Smoothing		Noise Reduced Using HSSNR	
		Is the Target Detected	Area Ratio	Is the Target Detected	Area Ratio	Is the Target Detected	Area Ratio
Awning	12mx12m	yes	0.83	yes	0.73	yes	0.99
	6mx6m	yes	0.94	yes	0.85	yes	1.07
	3mx3m	yes	0.65	marginally	0.20	yes	0.72
	1,5mx1,5m	yes	1.14	yes	0.81	yes	0.96
	1mx1m	yes	0.60	no	-1.52	yes	1.13
White Tarp	6mx6m	yes	0.87	no	0.00	yes	1.02
	3mx3m	yes	1.16	no	0.00	yes	1.35
	1mx1m	no	-0.18	no	0.00	yes	1.52
Cotton	6mx6m	no	0.00	no	0.00	yes	1.08
	3mx3m	no	0.00	no	0.00	marginally	0.30
	1mx1m	no	0.00	no	0.00	marginally	0.11
Vinyl Mat	11mx14m	yes	1.08	yes	1.12	yes	1.28

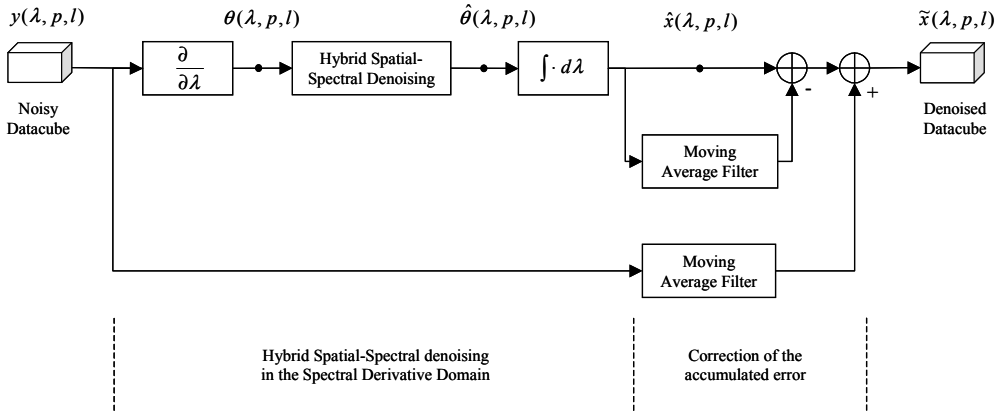

Figure 1. Block diagram of the hybrid spectral-spatial noise reduction (HSSNR) technology for hyperspectral data. (λ: a spectral band centre, p: cross-track pixel number, l: along-track line number).

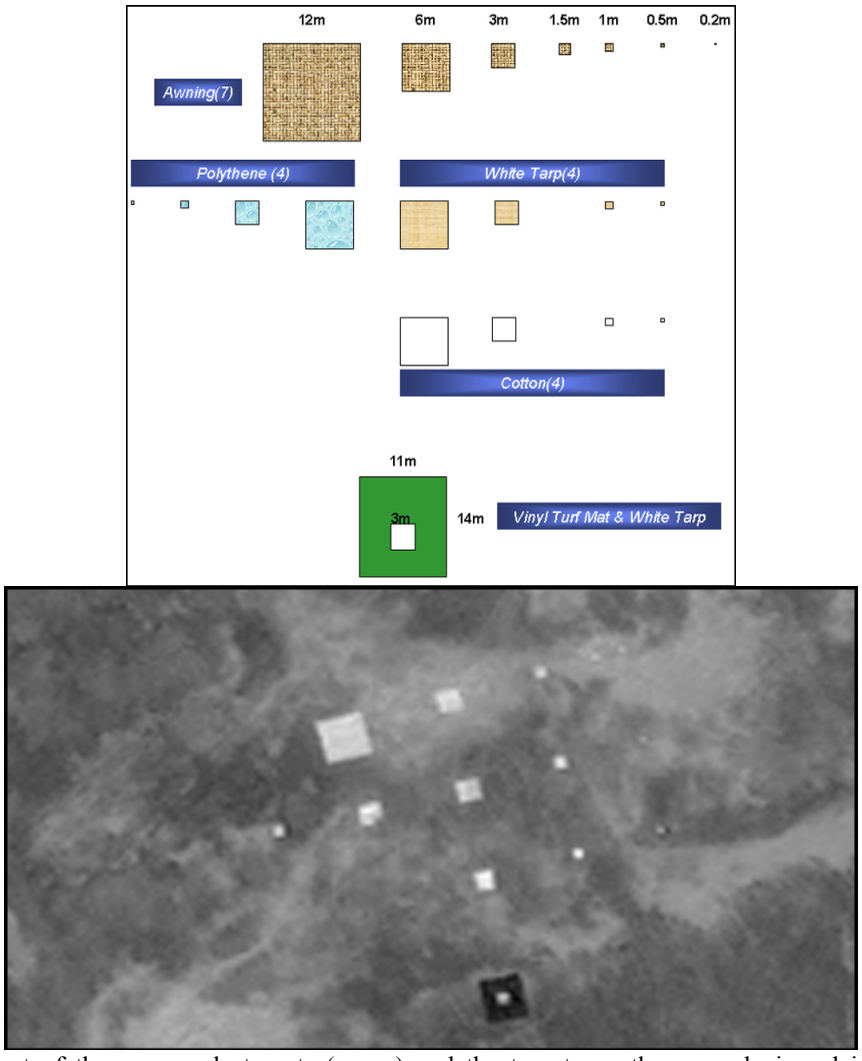

Figure 2. Layout of the man-made targets (upper) and the targets on the ground viewed in an IKONOS panchromatic scene (1 m resolution).

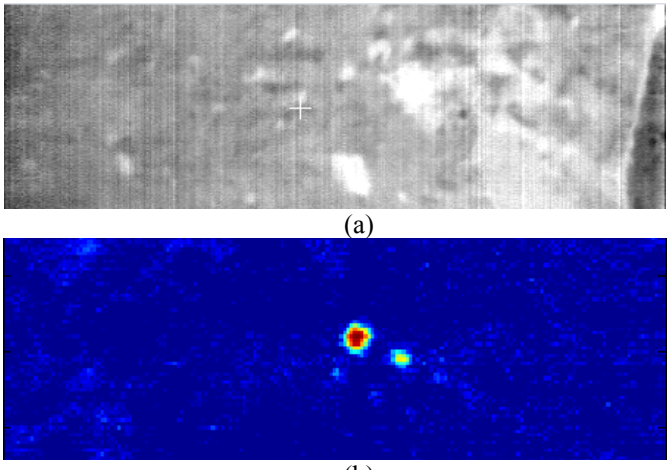

(a)

(b)

Figure 3 (a) Image of the SFSI-II datacube displayed in band 100 (1700nm) with linear contrast enhancement, (b) part of the fraction image of the awning material.

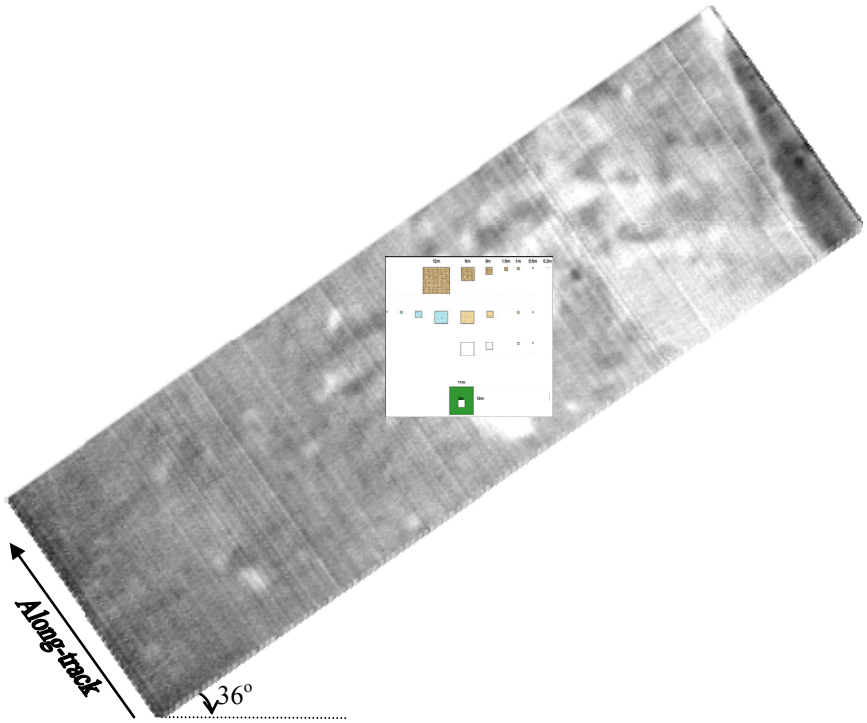

Figure 4 Disposition of the man-made target array in the scene of the SFSI-II datacube (there is a rotation angle of approximate 36° between the target array and the cross-track line of the SFSI-II datacube.).

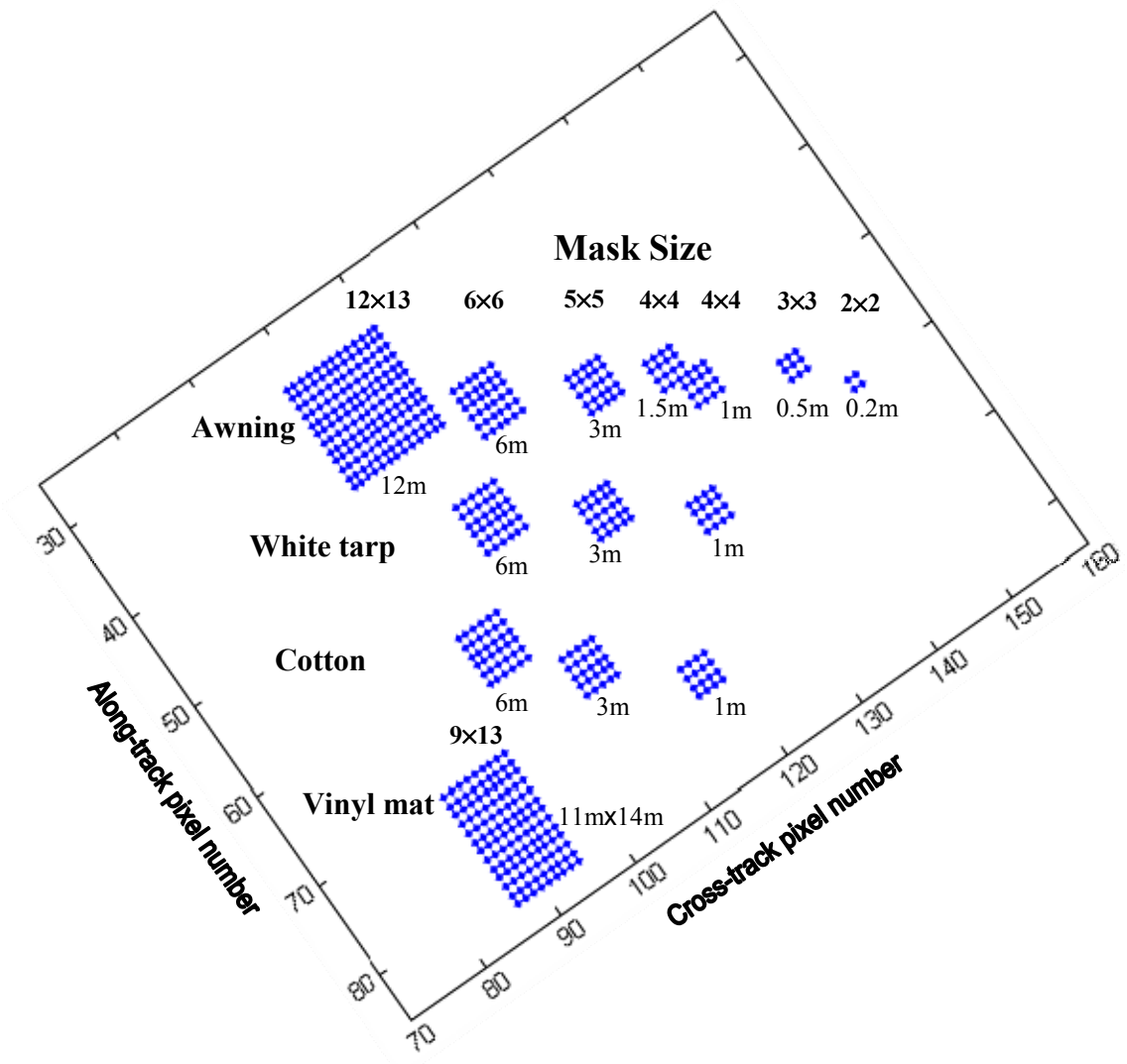

Figure 5 Locations and the sizes of the masks used in the evaluation of the derived targets from the SFSI-II datacube. The target array covered by the masks is matched with the target array in Figure 2.

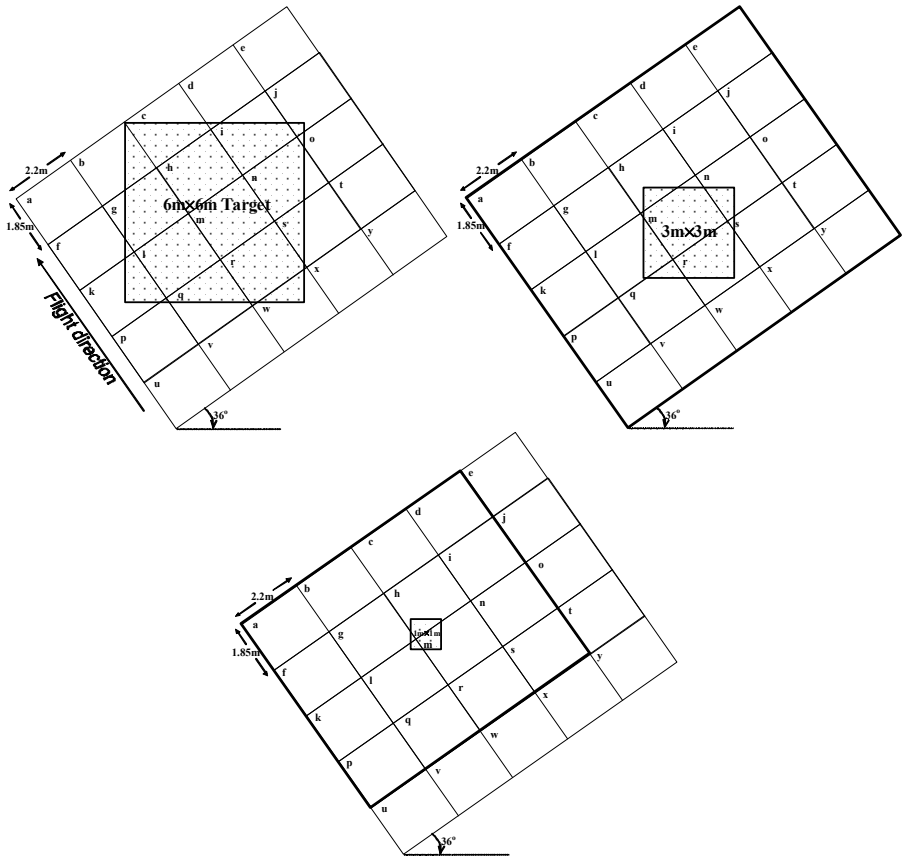

Figure 6. Ground pixels covered by a 6m×6m target (left graphics), a 3m×3m target (centre graphics) and a 1m×1m target (right graphics) in the scene of the SFSI-II datacube with the sensor's ground pixel size of 2.20m×1.85m and a rotation angle between the targets and the cross-track line of 36^{o}.

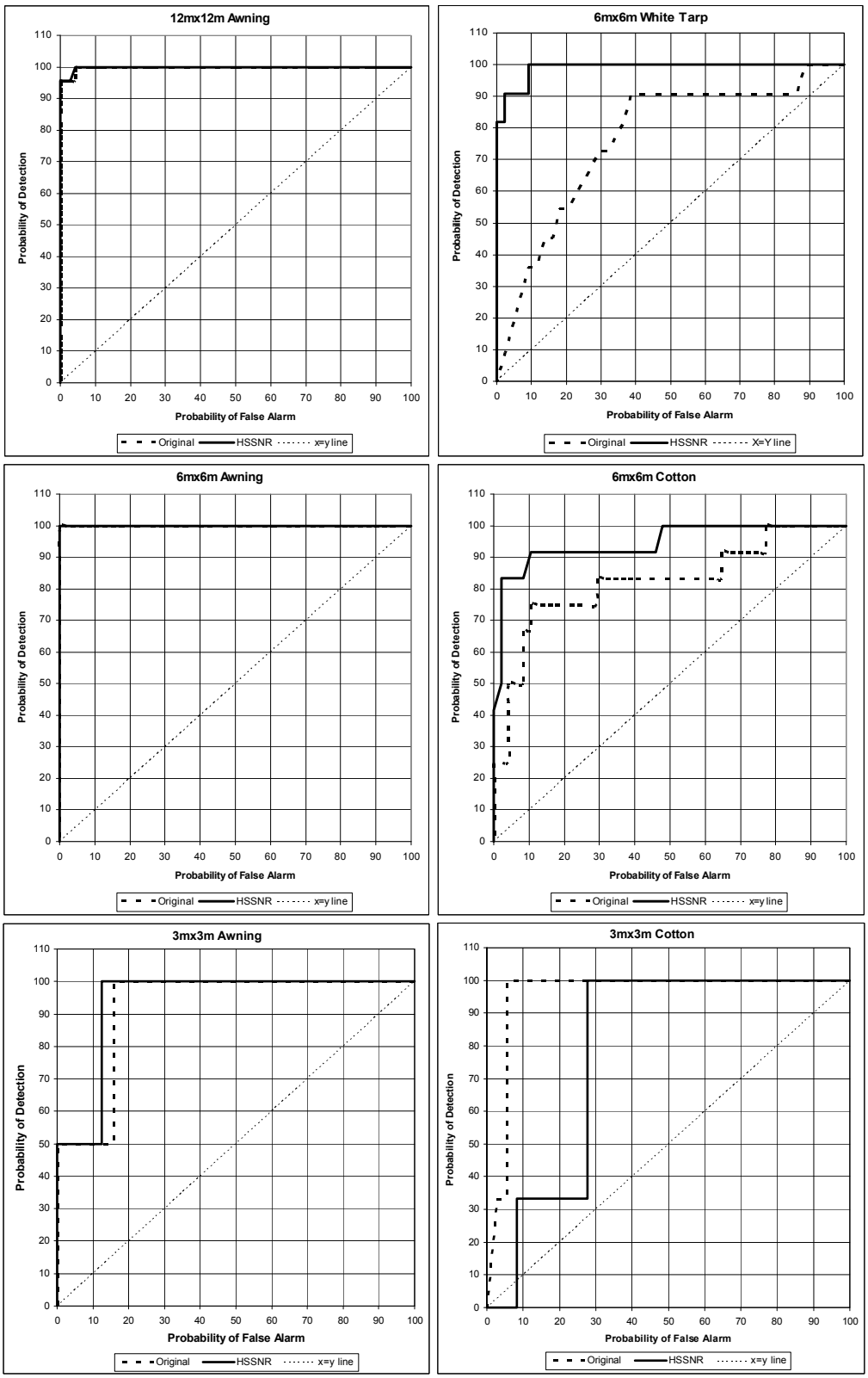

Figure 7. ROC curves of awning, white tarp and cotton targets of sizes from 12m×12m to 3m×3m derived from the original SFSI-II datacube and the HSSNR noise-reduced datacube.